Research Paper

An Under-Sampled Line Array Element Signal Reconstruction Method Based on Compressed Sensing Theory

Tongjing SUN*, Mengwei ZHOU, Lei CHEN

Department of Automation, Hangzhou Dianzi University
Hangzhou, China

*Corresponding Author e-mail: stj@hdu.edu.cn

The half-wavelength spacing arrangement of underwater uniform linear arrays has been widely used for better anti-interference performance and higher signal gain. However, practical challenges of small element spacing, numerous elements, high hardware costs, large data storage requirements, high processing complexity, and mutual coupling effects between elements, have hindered its widespread use. This paper proposes an under-sampled array signal reconstruction method based on the compressed sensing (CS) theory in the element domain. This method is not limited by the array configuration and constructs a deterministic measurement matrix that satisfies the restricted isometry property (RIP). Based on the array configuration, to ensure reconstruction performance. The method uses a two-dimensional orthogonal matching pursuit (OMP) method for time-space joint reconstruction of under-sampled spatial signals. Our simulation and practical test data processing results demonstrate that this method can achieve high-precision reconstruction of under-sampled array element domain signals at low under-sampling rates and can reconstruct full array signals with minimal error. Even under low signal-to-noise ratio (SNR) conditions, offering a practical and efficient solution to the challenges of underwater acoustic array signal processing.

Keywords: underwater acoustic array; compressed sensing; under-sampled array; signal reconstruction; deterministic measurement matrix.

1. Introduction

Array-based reception methods are usually used to resist interference and improve gain, including uniform linear arrays (ULA), uniform circular arrays (UCA), *L*-shaped arrays, and planar arrays (BALANIS, 2016; SILVER, 2019; ZHANG *et al.*, 2013). The ULA is the most common, featuring uniformly spaced array elements. Studies have shown that a ULA performs best when the spacing between array elements is half the wavelength. However, with the advent of large arrays such as towed line arrays, a larger array aperture is required to cover more spatial data. Using half-wavelength spacing necessitates an increasing number of array elements. For example, the number of elements can reach thousands for a ULA operating at 28 kHz with an array length of tens of meters. This leads to greater data storage requirements and increased processing complexity, exceeding active sonar systems' hardware and software processing capabilities, and thus affecting performance.

To address this issue, researchers have explored sparse arrays. Sparse arrays sample a subset of elements from a ULA, allowing the spacing between elements to exceed the half-wavelength limit, thereby reducing the number of elements while still achieving the desired performance. Nested arrays (PAL, VAIDYANATHAN, 2010) and coprime arrays (VAIDYANATHAN, PAL, 2011) are typical examples of sparse arrays. A coprime array is formed by interleaving two subarrays with coprime numbers of elements. In contrast, a nested array is created by nesting multiple levels of subarrays, with the spacing of each level determined by the number of elements in the previous level. Various improved sparse arrays have been proposed based on the concepts of nested and coprime arrays (HE *et al.*, 2022; MOHSEN *et al.*, 2023; YANG *et al.*, 2023). Sparse arrays are widely used in array signal processing because they increase the degrees of freedom. One approach is to use the difference coarray of a sparse array to construct an equivalent virtual ULA and then obtain the covariance matrix of the virtual ULA by vectorizing

the covariance matrix (Lei *et al.*, 2015; Li, Zhang, 2020; Kazarinov, 2022). However, this virtual domain method has limitations regarding the array configuration. If the difference coarray of a sparse array has holes, it increases the processing complexity.

The advent of compressed sensing (CS) theory has provided an effective means for array signal processing (Candès, Wakin, 2008; Ender, 2010). The core idea is to take advantage of the signal sparsity to reduce the amount of sampled data, which has been extensively applied in processing under-sampled signals in the time domain (Li, Yang, 2014; Jurdana *et al.*, 2023). Since signal sources are sparse in the spatial domain, naturally satisfying the sparsity requirement of CS, it has also been applied to signal reconstruction in the spatial domain. Mirza *et al.* (2020) have proposed a CS technique based on a sparse array for direction of arrival (DOA) estimation, addressing grid mismatch issues in spatial CS, thereby enhancing the robustness of CS DOA techniques. Kikuchi *et al.* (2022) applied CS theory to process ULA, effectively reducing the number of elements in antenna arrays. The measurement matrices used in these studies are random. Although the random measurement matrices satisfied the restricted isometry property (RIP) and yielded satisfactory results in reconstruction accuracy, it is impossible to determine the configurations of the sparse arrays obtained by sampling, thus hindering engineering implementation. For deterministic measurement matrices, Salama (2020), Lakshmi *et al.* (2021), and Chen *et al.* (2020) used the difference co-array of nested arrays to construct an equivalent ULA and vectorized the covariance matrix of the sparse array to reconstruct the ULA's received signal. However, these methods only reconstruct the covariance matrix of the ULA's received signal and cannot reconstruct the received signal in the element domain.

This paper applies CS theory to the reconstruction of element-domain signals. By constructing a sensing matrix and using a two-dimensional orthogonal matching pursuit (OMP) method, the time-domain signals are projected onto the element domain to achieve the reconstruction of under-sampled array signals. This approach imposes fewer restrictions on the array configurations of sparse arrays for signal reconstruction. Furthermore, reconstructing signals in the element domain allows sampling only a portion of the array elements to obtain the entire array's received data, effectively reducing the data storage requirements for large arrays.

2. Compressed sensing theory

For sparse signals, CS theory samples signals at a rate much lower than the Nyquist sampling theorem to obtain discrete samples of the original signals. These samples are then used to reconstruct the original signals through reconstruction algorithms. If a signal can be sparsely represented, a measurement matrix unrelated to the transformation basis can be designed to observe it. The observed values can then be used to achieve exact or approximate signal reconstruction by solving optimization problems. The process mainly includes two parts: CS observation and signal reconstruction.

2.1. Compressed sensing observation part

Consider an N-dimensional discrete-time domain signal $\mathbf{X}$ and an $N \times N$-dimensional sparse representation matrix $\mathbf{\Psi}$, consisting of $N \times N$-dimensional basis vectors. If the signal $\mathbf{X}$ can be represented as

$$\mathbf{X} = \sum_{i=1}^{N} \mathbf{\psi}_i \alpha_i = \mathbf{\Psi}\,\boldsymbol{\alpha}, \tag{1}$$

where $\boldsymbol{\alpha}$ is a sparse vector containing only K ($K \ll N$) non-zero values, this implies that $\mathbf{X}$ can be sparsely represented. Then, a measurement matrix $\mathbf{\Phi} \in R^{M \times N}$ ($M \ll N$) that satisfies certain conditions is used to "sense" the signal, resulting in an M-dimensional observation signal of $\mathbf{X}$:

$$\mathbf{Y} = \mathbf{\Phi}\,\mathbf{X}. \tag{2}$$

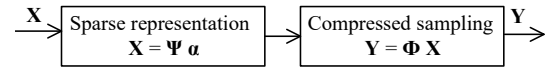The process of CS observation is illustrated in Fig. 1.

Fig. 1. Process of CS observation.

2.2. Signal reconstruction sections

After obtaining the linear observation vector $\mathbf{Y}$ of the signal $\mathbf{X}$ with respect to the measurement matrix $\mathbf{\Phi}$, the next step is to determine how to recover $\mathbf{X}$ from $\mathbf{Y}$. Since directly solving the underdetermined Eq. (2) is infeasible, we use the sparse representation of $\mathbf{X}$ in Eq. (1):

$$\mathbf{Y} = \mathbf{\Phi}\,\mathbf{X} = \mathbf{\Phi}\,\mathbf{\Psi}\,\boldsymbol{\alpha} = \mathbf{\Theta}\,\boldsymbol{\alpha}, \tag{3}$$

where $\mathbf{\Theta} = \mathbf{\Phi}\,\mathbf{\Psi}$ is a $M \times N$-dimensional matrix called the sensing matrix. We can think of $\mathbf{Y}$ as the projection of $\boldsymbol{\alpha}$ onto the sensing matrix $\mathbf{\Theta}$. Thus, the problem now becomes recovering $\boldsymbol{\alpha}$ from $\mathbf{Y}$. Although Eq. (3) is also an underdetermined equation, the sparsity of $\boldsymbol{\alpha}$ significantly reduces the number of unknowns, making signal reconstruction feasible.

Candès and Wakin (2008) proved that, under the condition that the signal $\boldsymbol{\alpha}$ is sparse, if the sensing matrix $\mathbf{\Theta}$ satisfies the condition that any $2K$ columns are linearly independent, the solution can be obtained using the following equation:

$$\begin{cases} \widehat{\alpha} = \arg\min \|\boldsymbol{\alpha}\|_0, \\ \text{subject to } \mathbf{\Theta}\boldsymbol{\alpha} = \mathbf{Y}. \end{cases} \tag{4}$$

Equation (4) is an NP-hard non-convex optimization problem, making it very challenging to solve. Numerous optimization algorithms have been proposed to address this issue (Zhao, Nehorai, 2014; Wang *et al.*, 2022). After recovering $\boldsymbol{\alpha}$ through the reconstruction algorithm, the signal $\mathbf{X}$ can be reconstructed according to Eq. (1).

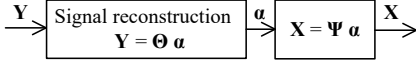The process of signal reconstruction can be illustrated in Fig. 2.

Fig. 2. Process of CS reconstruction signal.

From the aforementioned analysis, it can be concluded that the primary research focus of CS encompasses the following three aspects:

1) sparse representation: designing a sparse representation matrix to represent the original signal $\mathbf{X}$ as a sparse vector $\boldsymbol{\alpha}$ of the same length;

2) compressed sampling: using an $M \times N$ measurement matrix, CS observes the high-dimensional original signal $\mathbf{X}$ to obtain the low-dimensional observed signal $\mathbf{Y}$;

3) signal reconstruction: recovering the original signal $\mathbf{X}$ from the observed signal $\mathbf{Y}$ by solving Eq. (4).

3. Under-sampled array signal reconstruction method in the element domain

The application of CS in the time domain mainly deals with one-dimensional signals. However, array reception signals are typically two-dimensional, encompassing both the element domain (spatial domain)

and the time domain. Focusing on the three critical technologies of sparse representation, compressed sampling, and signal reconstruction, this paper uses the inherent sparsity of spatial arrays, constructing a sparse matrix from steering vectors of various angles for sparse representation in the spatial domain. Based on the configuration of the under-sampled array, a measurement matrix satisfying the RIP condition is constructed using a unit diagonal sampling method. It extends the OMP method to the two-dimensional space-time joint domain for signal reconstruction in the element domain. The implementation process is shown in Fig. 3.

3.1. Sparse representation of array signals

CS requires the original signal to be sparsely representable. When applied to the element domain, the target is sparse in the spatial domain, naturally satisfying the sparsity condition.

Suppose a ULA with N hydrophones spaced by d receives K signals with identical central frequency f_0 and wavelength λ. We first consider the case of a single snapshot, where the time-domain signal received by the array can be described as

$$\mathbf{X} = \mathbf{A}\,\mathbf{s} + \mathbf{N}, \tag{5}$$

where $\mathbf{X} = [\mathbf{x}_1, \mathbf{x}_2, ..., \mathbf{x}_N]^{\mathrm{T}}$, $\mathbf{N} = [\mathbf{n}_1, \mathbf{n}_2, ..., \mathbf{n}_N]^{\mathrm{T}}$, $\mathbf{x}_N$, $\mathbf{n}_N$, respectively, represent the signal and additive noise received by the N-th array element. Additionally, $\mathbf{s} = [\mathbf{s}_1, \mathbf{s}_2, ..., \mathbf{s}_K]^{\mathrm{T}}$, where $\mathbf{s}_K$ represents the K-th incident signal on the array. The matrix $\mathbf{A}$ is the $N \times K$-dimensional array manifold matrix:

$$\mathbf{A} = [\mathbf{a}(\theta_1), \mathbf{a}(\theta_2), ..., \mathbf{a}(\theta_k)]^{\mathrm{T}}, \tag{6}$$

where $\mathbf{a}(\theta_k)$ is the steering vector of the array in the direction θ_k:

$$\mathbf{a}(\theta_k) = \left[1, \exp\left(-\frac{j2\pi\,\mathrm{d}\sin(\theta_k)}{\lambda}\right), \exp\left(-j2\pi \cdot \frac{2\,\mathrm{d}\sin(\theta_k)}{\lambda}\right), ..., \exp\left(-j2\pi \cdot \frac{2\,\mathrm{d}\sin(\theta_k)}{\lambda}\right)\right]^{\mathrm{T}}. \tag{7}$$
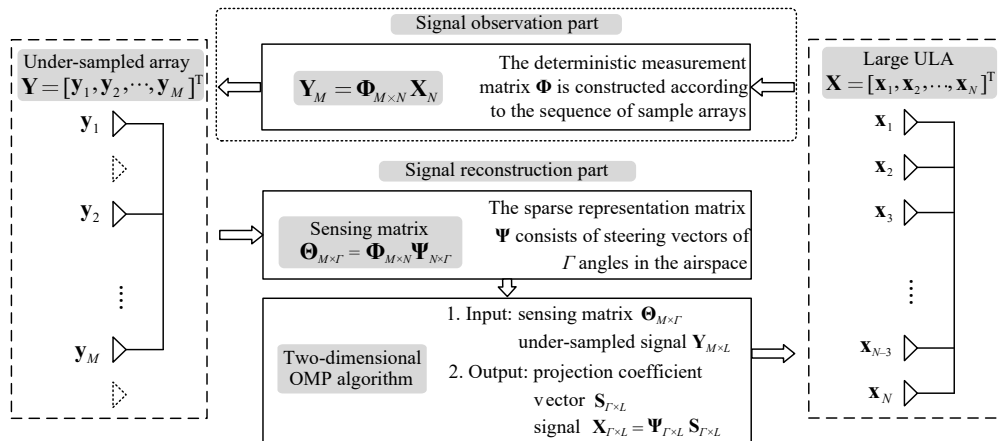

Fig. 3. Flow chart of signal reconstruction method of under-sampled array.

If the spatial domain from $-90°$ to $90°$ is divided into Γ grids, and the incident angles of the K signal sources fall on these grids, we obtain Γ spatial angles. The array steering vectors at these Γ angles are used to form an extended array manifold matrix $\boldsymbol{\Psi}$. Thus, Eq. (5) can be further expressed as:

$$\mathbf{X} = \boldsymbol{\Psi}\,\mathbf{s} + \mathbf{N}, \tag{8}$$

where $\mathbf{s}$ is a Γ-dimensional projection coefficient vector, and each element of $\mathbf{s}$ corresponds to a grid. Since there are only K grids with incident signals among the Γ grids, $\mathbf{s}$ is a K-sparse vector, having a form similar to $[0, 0, ..., \mathbf{s}_1, 0, ..., 0, ..., \mathbf{s}_K, 0, ...0]^{\mathrm{T}}$, where non-zero values occur only at the grids with incident signals.

Equation (8) shows that the array received signal $\mathbf{X}$ is sparsely represented as a sparse vector $\mathbf{s}$ through the extended array manifold matrix $\boldsymbol{\Psi}$. The extended array manifold matrix $\boldsymbol{\Psi}$ serves as the sparse representation matrix, constructed through the following steps:

1) divide the spatial domain from $-90°$ to $90°$ into Γ grids of equal angles, resulting in $\{\theta_1, \theta_2, ..., \theta_\Gamma\}$;
2) obtain the steering vectors of the array at these Γ angles: $\{\mathbf{a}\,(\theta_k)\}_{k=1}^{\Gamma}$;
3) form the sparse representation matrix: $\boldsymbol{\Psi} = [\mathbf{a}\,(\theta_1), \mathbf{a}\,(\theta_2), ..., \mathbf{a}\,(\theta_\Gamma)]^{\mathrm{T}}$.

3.2. Construction of the measurement matrix based on under-sampled array configuration

In CS, the under-sampling of large ULAs is achieved through a measurement matrix. The critical difference between element-domain CS and time-domain CS is that the measurement matrix of element-domain CS does not require a linear combination of all element signals for compressive sampling. From a hardware perspective, linear combination of element signals still necessitates sampling each element. However, the under-sampled signals we obtain only contain the received signals from a subset of elements.

In the element domain, the received signal of an N-element ULA can be expressed as $\mathbf{X} = [\mathbf{x}_1, \mathbf{x}_2, ..., \mathbf{x}_N]^{\mathrm{T}}$, where $\mathbf{x}_i$ $(i = 1, 2, ..., N)$ is the signal received by the i-th element. The measurement matrix $\boldsymbol{\Phi}$ consists of $M \times N$-dimensional sampling basis vectors $\boldsymbol{\varphi}_i$ $(i = 1, 2, ..., M)$, each of which samples the original array signal $\mathbf{X}$ once, obtaining one element signal. In total, the M sampling basis sample M element signals, forming the under-sampled array signal $\mathbf{Y} = [\mathbf{y}_1, \mathbf{y}_2, ..., \mathbf{y}_M]^{\mathrm{T}}$. To ensure that each sampling basis samples only one element, each N-dimensional sampling basis vector can be a sparse vector containing only one non-zero value. Moreover, to avoid redundant sampling, the positions of the non-zero values in the M sampling basis should be different.

Figure 4 illustrates the process of element signal under-sampling. By sorting the M sampling basis vectors according to the positions of their non-zero values, the measurement matrix has a structure similar to that of Eq. (9). It can be viewed as M rows extracted from an identity diagonal matrix, where the columns are linearly independent, ensuring that the resulting measurement matrix satisfies the RIP:

$$\boldsymbol{\Phi} = \begin{pmatrix} 1 & 0 & 0 & & 0 & 0 & 0 \\ 0 & 0 & 1 & \cdots & 0 & 0 & 0 \\ & \vdots & & \ddots & & \vdots & \\ 0 & 0 & 0 & & 1 & 0 & 0 \\ 0 & 0 & 0 & \cdots & 0 & 1 & 0 \end{pmatrix}. \tag{9}$$

Thus, the steps to construct the measurement matrix are as follows:

1) determine the positions of the sampled elements in the under-sampled array: $D = [d_1, d_2, ..., d_M]$;
2) construct an N-dimensional identity diagonal matrix $\mathbf{E}$;
3) extract the i-th rows from $\mathbf{E}$ to form the measurement matrix $\boldsymbol{\Phi}$.

3.3. Signal reconstruction based on two-dimensional OMP

Subsections 3.1 and 3.2 discussed the mathematical model for the single snapshot case. Now, we consider
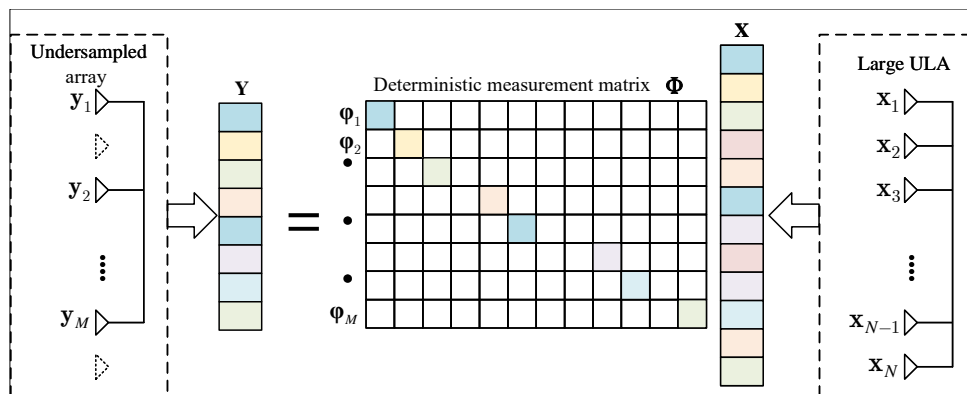

Fig. 4. Signal compression sampling in the element domain.

the scenario with L snapshots. The problem of reconstructing the original $N \times L$-dimensional array signal X from the $M \times L$-dimensional array signal $\mathbf{Y}$ can be described as

$$\begin{cases} \widehat{\mathbf{S}} = \arg\min \|S\|_0, \\ X = \mathbf{\Psi}\widehat{\mathbf{S}}, \\ \text{subject to} \quad \mathbf{\Theta}\mathbf{S} = \mathbf{Y}, \end{cases} \tag{10}$$

where $\widehat{\mathbf{S}}$ is an $M \times L$ matrix containing L projection coefficient vectors; $\mathbf{\Psi}$ is an $N \times \Gamma$-dimensional sparse representation matrix, and $\mathbf{\Theta}$ is an $M \times \Gamma$ sensing matrix obtained by $\mathbf{\Theta} = \mathbf{\Phi}\mathbf{\Psi}$, with $\mathbf{\Phi}$ being the measurement matrix as detailed in Subsec. 3.2.

The reconstruction of the one-dimensional projection coefficient vector involves solving the problem in Eq. (4). In CS, there are numerous optimization algorithms available to solve Eq. (4). The OMP algorithm is one such reconstruction method, which uses an iterative approach to obtain the solution (Tropp, Gilbert, 2007). However, traditional OMP cannot handle two-dimensional signals as presented in Eq. (10). This paper utilizes a two-dimensional OMP algorithm. The under-sampled signal $\mathbf{Y}$ is first divided into L vectors by columns, and then each vector is sequentially solved:

$$\begin{cases} \widehat{\mathbf{s}}_i = \arg\min \|\mathbf{s}_i\|_0, \\ \text{subject to} \quad \mathbf{\Theta}\mathbf{s} = \mathbf{Y}_i, \end{cases} \tag{11}$$

where $\mathbf{Y}_i$ denotes the i-th column of $\mathbf{Y}$, and $\widehat{\mathbf{s}}_i$ represents the projection coefficient vector reconstructed from it. Finally, the L projection coefficient vectors form the projection coefficient matrix $\widehat{\mathbf{S}}$.

The two-dimensional OMP algorithm process is as follows:

1) initialize the projection coefficient matrix $\mathbf{S}_{\Gamma \times L}$ and set the iteration count $i = 1$. repeat steps (2) to (4) L times until $i > L$, then proceed to step (5);

2) initialize the projection coefficient vector $\boldsymbol{\alpha}_\Gamma$, residual $\mathbf{r}_0 = \mathbf{Y}_i$, index set $\Lambda_0 = \varnothing$, and inner loop iteration count $n = 1$. Repeat steps (a) to (e) until the stopping criterion is met:

   a) find the atom column in $\mathbf{\Theta}$ most correlated with the residual and its index:

   $$\lambda_n = \arg\max_{j \notin \Lambda_{n-1}} \|\langle \theta_j, \mathbf{r}_{n-1}\rangle\|,$$

   where θ_j is the j-th column of $\mathbf{\Theta}$;

   b) update the index set: $\Lambda_n = \Lambda_{n-1} \cup \lambda_n$;

   c) solve the projection coefficient vector using least squares:

   $$\mathbf{s}_n(t \in \Lambda_n) = \arg\min_x \|\mathbf{\Theta}_{\Lambda_n} x - \mathbf{Y}_i\|_2,$$

   $$\mathbf{s}_n(t \notin \Lambda_n) = 0;$$

   d) update the residual: $\mathbf{r}_n = \mathbf{r}_{n-1} - \mathbf{\Theta}\mathbf{s}_n$;

   e) $n = n + 1$;

3) output the projection coefficient vector $\mathbf{s}$ as the i-th row of $\mathbf{S}_{\Gamma \times L}$;

4) $i = i + 1$;

5) recover the signal: $\mathbf{X}_{N \times L} = \mathbf{\Psi}_{N \times \Gamma}\mathbf{S}_{\Gamma \times L}$.

Using the two-dimensional OMP algorithm, the entire array signal $\mathbf{X}$ is reconstructed from the under-sampled array signal $\mathbf{Y}$.

4. Performance verification based on simulated and measured data

This section compares the reconstruction error under different under-sampling rates, array configurations, and signal-to-noise ratio (SNR) using simulated and measured data. For an N-element ULA, M elements are sampled. When $M < N$, the array is under-sampled, and the ratio M/N is the under-sampling rate. The reconstruction error is defined as

$$\text{Error} = \frac{\|\widehat{\mathbf{X}}_{N \times L} - \mathbf{X}_{N \times L}\|_2}{\|\mathbf{X}_{N \times L}\|_2}, \tag{12}$$

where $\widehat{\mathbf{X}}_{N \times L}$ is the reconstructed signal, and $\mathbf{X}_{N \times L}$ is the original signal.

4.1. Performance verification using simulated data

The simulation involves the transmission of linear frequency-modulated signals by active sonar with a center frequency of 28 kHz and a bandwidth of 16 kHz. A 32-element ULA receives the echo signal. The full array signal received by the ULA is the original signal $\mathbf{X}$. The under-sampled signal $\mathbf{Y}$ is obtained using the constructed measurement matrix as described Eq. (2). The measurement matrix can be either deterministic, as shown is Subsec. 3.2, or random. The underwater sound speed is set to $c = 1500$ m/s, and the element spacing is half the wavelength of the echo signal.

4.1.1. Signal waveform comparison

In this section, the waveform of the original signal from unsampled elements is compared with the reconstructed signal at an under-sampling rate of 50 % and SNR = 5 dB. The positions of the 16 sampled elements are $\{1, 2, 3, 5, 10, 11, 15, 16, 17, 19, 22, 23, 24, 25, 31, 32\}$. The original and reconstructed signals from the 18th and 28th elements among the remaining 16 unsampled elements are compared, as shown in Fig. 5.

4.1.2. Reconstruction error of different under-sampled arrays

In this section, at an under-sampling rate of 50 % and SNR = 5 dB, 100 sets of under-sampled structures
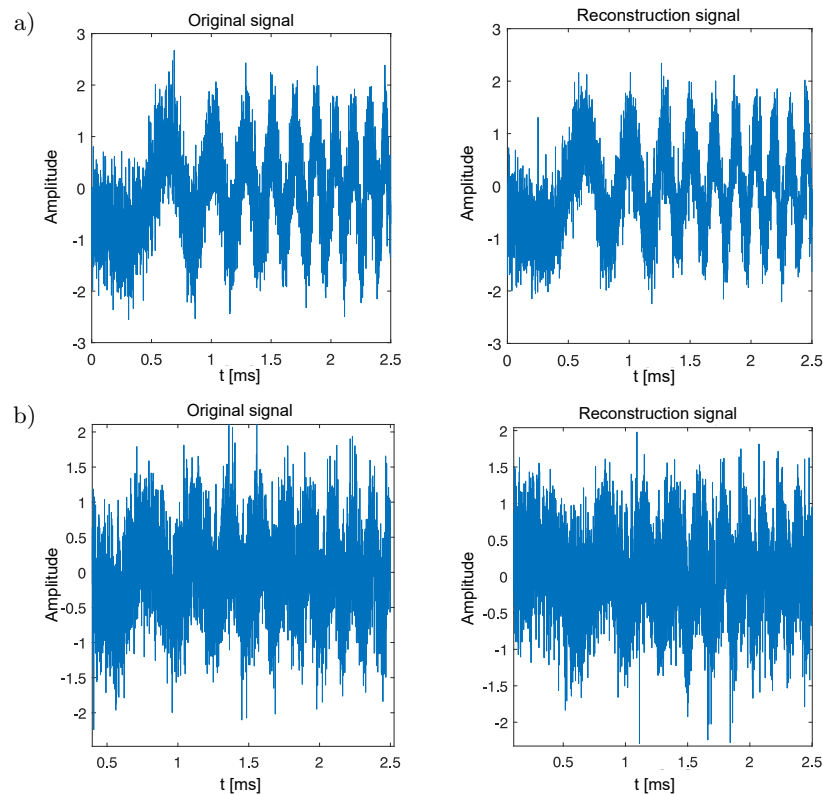
Fig. 5. Comparison of signal waveforms before and after reconstruction: a) the 18th element; b) the 28th element.

are independently tested using a random measurement matrix. Each set of structures undergoes five repeated experiments, and the average reconstruction error of the five experiments is taken as the reconstruction error for that set. The results are shown in Fig. 6, with reconstruction errors mainly ranging from 0.1 to 0.25, and some under-sampled structures exhibiting large errors.
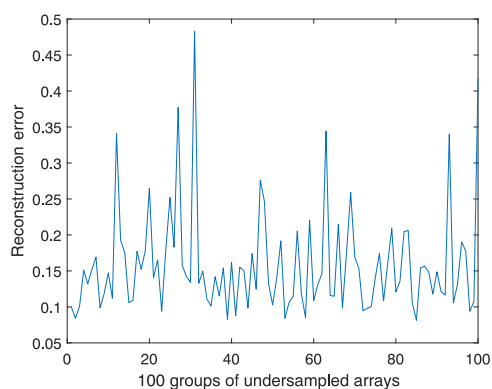

Fig. 6. Reconstruction errors of different under-sampled arrays.

4.1.3. Reconstruction error at different under-sampling rates

Five sets of under-sampled arrays are selected, and the under-sampling rates are gradually reduced from 87.5 % to 12.5 % by removing one redundant element

from the under-sampled array each time, while keeping other conditions unchanged. The reconstruction error at different under-sampling rates is then compared. Each set of under-sampled arrays undergoes five repeated experiments to avoid randomness, and the average error is computed. The results are shown in Table 1. From Table 1, it can be seen that when the under-sampling rate reaches 31.25 % or higher, the reconstruction error is generally below 0.2, indicating good reconstruction effect.

Table 1. Reconstruction errors of five under-sampled arrays at different under-sampling rates.

Under-sampling rate	25 %	31.25 %	37.5 %	50 %	75 %	87.5 %
1	0.702	0.151	0.14	0.094	0.071	0.063
2	0.677	0.124	0.109	0.102	0.069	0.062
3	0.895	0.124	0.1	0.081	0.055	0.059
4	0.47	0.23	0.195	0.165	0.078	0.068
5	0.528	0.265	0.251	0.185	0.095	0.061

4.1.4. Reconstruction error under different SNR

Ten groups of under-sampled arrays are selected to construct deterministic measurement matrices. Each group undergoes an independent experiment at an under-sampling rate of 50 %. The reconstruction performance under different SNRs is then analyzed. Each group of under-sampled arrays is subjected to five re-

peated experiments to avoid randomness. The results are shown in Table 2. It can be observed that high SNRs yield lower reconstruction errors. For signals without noise, the optimal reconstruction error can reach 0.009, which is almost negligible.

Table 2. Reconstruction errors of five under-sampled arrays under different SNR.

SNR [dB]	1	2	3	4	5
Noise is 0	0.066	0.011	0.094	0.009	0.009
5	0.079	0.115	0.155	0.111	0.095
7	0.067	0.095	0.133	0.064	0.080
10	0.05	0.074	0.114	0.048	0.067
15	0.055	0.047	0.097	0.035	0.051

4.2. Performance verification using measured data

The measured data is obtained from a lake test at the Xin'anjiang test site, where the underwater sound speed is approximately 1450 m/s. A linear frequency modulated signal with a frequency range of 20 kHz– 36 kHz is transmitted with a pulse width of 2 ms. The test setup is shown in Fig. 7. A 32-element ULA receives the underwater echo signal, sampled at 1 MHz. The hydrophone array and target are 10 m underwater, and the transmitter is 9.5 m underwater. The target is a 0.6 m diameter spherical model.

Due to the complexity of the underwater environment, and to more clearly observe the target, we apply a matched filter to both the original signal $\mathbf{X}$ and the reconstructed signal $\widehat{\mathbf{X}}$, resulting in $\mathbf{X}'$ and $\widehat{\mathbf{X}}'$, respectively. Then, the reconstruction error is calculated using Eq. (13):

$$\text{Error} = \frac{\left\| \widehat{\mathbf{X}}'_{N \times L} - \mathbf{X}'_{N \times L} \right\|_2}{\left\| \mathbf{X}'_{N \times L} \right\|_2}, \tag{13}$$

where $\widehat{\mathbf{X}}'_{N \times L}$ is the matched filter signal of the reconstructed signal $\widehat{\mathbf{X}}_{N \times L}$, and $\mathbf{X}'_{N \times L}$ is the matched filter signal of the original signal $\mathbf{X}_{N \times L}$.

4.2.1. Signal waveform comparison

In this section, the 32-element ULA is processed at a 75 % under-sampling rate. The positions of the sampled elements are selected as {1, 2, 3, 4, 5, 7, 8, 10, 12, 13, 14, 15, 16, 17, 18, 19, 21, 22, 26, 27, 28, 29, 30, 32}. Among the remaining eight unsampled elements, the signals before and after reconstruction at the 23th element are compared along with the results of matched filter. The results are shown in Fig. 8.

4.2.2. Reconstruction error of different under-sampled arrays

This section processes the measured data at a 75 % under-sampling rate. One hundred groups of under-sampled arrays are sampled using a random measurement matrix. The results are shown in Fig. 9, where the reconstruction error fluctuates between 0.08 and 0.28.

4.2.3. Reconstruction errors of 10 under-sampled arrays

Five groups of under-sampled arrays are selected. Starting with an under-sampling rate of 87.5 %, redundant elements are gradually removed to reduce the under-sampling rate to 37.5 % while keeping other conditions unchanged. The reconstruction error at different under-sampling rates is compared. The results are shown in Table 3. As shown in Table 3, the proposed algorithm achieves optimal performance with measured data, with reconstruction errors below 0.1 when the under-sampling rate is above 50 %.

Table 3. Reconstruction errors of five groups of under-sampled arrays at different under-sampling rates.

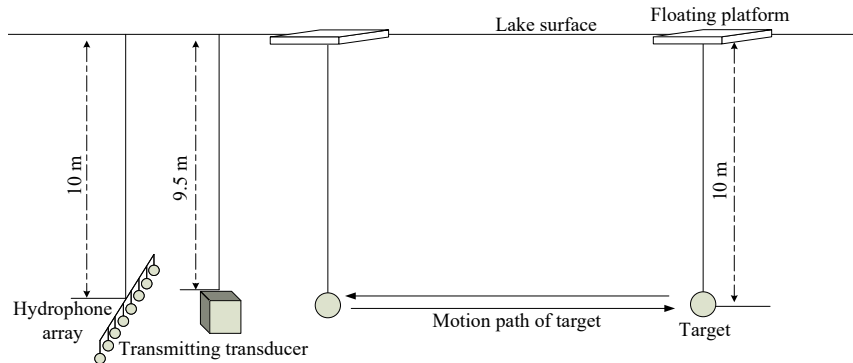| Under-sampling rate	37.5 %	50 %	62.5 %	75 %	87.5 %
1	0.164	0.103	0.071	0.064	0.083
2	0.174	0.117	0.096	0.092	0.107
3	0.166	0.099	0.086	0.076	0.095
4	0.157	0.116	0.085	0.079	0.099
5	0.166	0.125	0.097	0.096	0.106

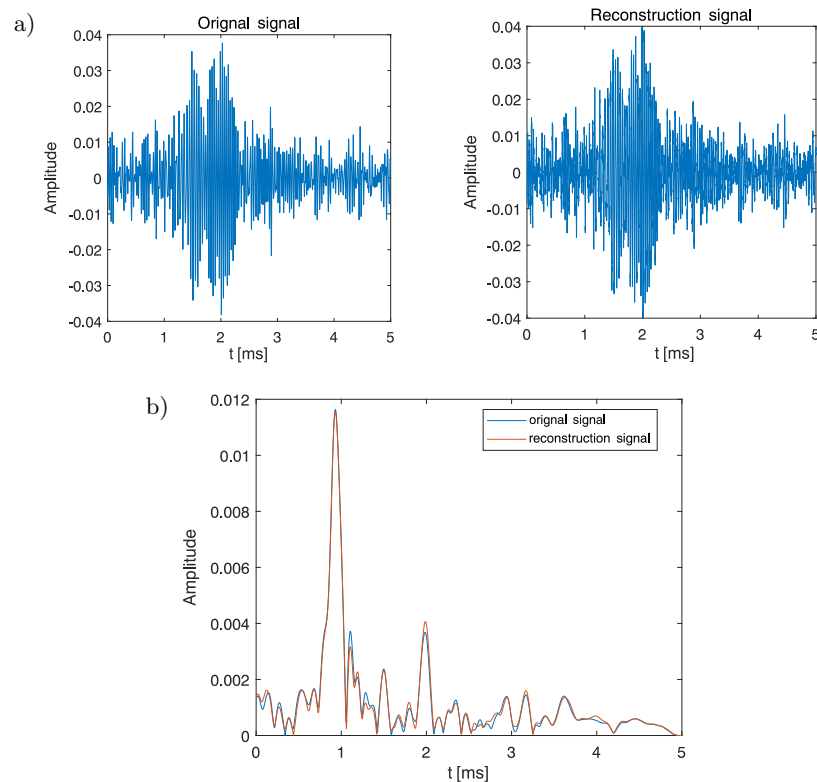Fig. 7. Experimental setup on the lake.

Fig. 8. Waveform comparison before and after reconstruction of measured data: a) signal comparison before and after reconstruction; b) comparison of matched filter results before and after reconstruction.
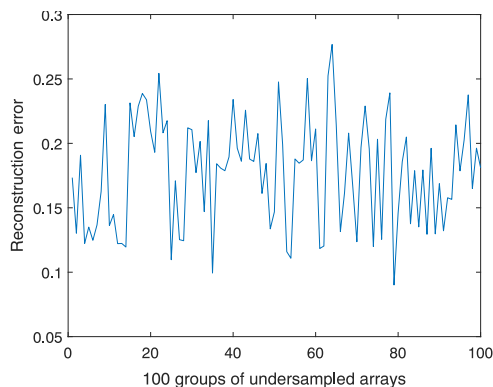

Fig. 9. Reconstruction error under different under-sampled arrays.

5. Conclusion

This paper addressed the under-sampling problem in large ULAs by applying CS theory to element-domain signal processing. The array signals were sparsely represented by exploiting the sparsity of signal sources in the spatial domain. Time-domain signals were projected onto the element domain through sparse representation. Then, reconstruction algorithms were used in the element domain to recover the full array signal from the under-sampled array signals. Compared to the method of reconstructing the original array covariance matrix, the element-domain signal reconstruction method directly processes the signal and

has broader applicability. Using CS for signal reconstruction allows recovering full array data from any under-sampled array, enabling data reception from redundant elements in large arrays without the need to sample them. The performance of this method is verified through the processing of both simulated and measured data, demonstrating that it can reconstruct element-domain signals with small errors even at low SNRs and varying under-sampling rates.

Acknowledgments

Declaration of competing interest

The authors declare that they have no known competing financial interests or personal relationships that could have influenced the work reported in this paper.

References

1. BALANIS C.A. (2016), *Antenna Theory: Analysis and Design*, 4th ed., John Wiley & Sons, New Jersey.

2. CANDÈS E.J., WAKIN M.B. (2008), An introduction to compressive sampling, *IEEE Signal Processing Magazine*, **25**(2): 21–30, https://doi.org/10.1109/MSP.2007.914731.

3. CHEN L.H., MA X.C., LI X., SONG Q.Y. (2020), Sparse array beamforming method combined with compressed sensing model [in Chinese], *Journal of Signal Processing*, **36**(4): 475–485, https://doi.org/10.16798/j.issn.1003-0530.2020.04.001.

4. ENDER J.H.G. (2010), On compressive sensing applied to radar, *Signal Processing*, **90**(5): 1402–1414, https://doi.org/10.1016/j.sigpro.2009.11.009.

5. HE J., TANG M., SHU T., YU W.X. (2022), Linear coprime sensor location arrays: Mutual coupling effect and angle estimation [in Chinese], *Journal of Electronics & Information Technology*, **44**(8): 2852–2858, https://doi.org/10.11999/JEIT210489.

6. JURDANA V., LOPAC N., VRANKIC M. (2023), Sparse time-frequency distribution reconstruction using the adaptive compressed sensed area optimized with the multi-objective approach, *Sensors*, **23**(8): 4148, https://doi.org/10.3390/s23084148.

7. KAZARINOV A.S. (2022), DOA estimation with sparse virtual arrays, [in:]*2022 Conference of Russian Young Researchers in Electrical and Electronic Engineering (ElConRus)*, pp. 1359–1362, https://doi.org/10.1109/ElConRus54750.2022.9755489.

8. KIKUCHI H., HOBARA Y., USHIO T. (2022), Compressive sensing to reduce the number of elements in a linear antenna array with a phased array weather radar, *IEEE Transactions on Geoscience and Remote Sensing*, **60**: 1–10, https://doi.org/10.1109/TGRS.2022.3152998.

9. LAKSHMI S., KUMAR N.S., HARI C.V., SRINATH S.A. (2021), Localization of underwater acoustic target using compressive sensing on nested array, [in:] *2021 Fourth International Conference on Microelectronics, Signals & Systems (ICMSS)*, pp. 1–5, https://doi.org/10.1109/ICMSS53060.2021.9673646.

10. LEI Y., WEI Y. S., LIU W. (2015), A novel adaptive beamforming technique for large-scale arrays, [in:] *2015 IEEE International Symposium on Signal Processing and Information Technology (ISSPIT)*, pp. 269–273, https://doi.org/10.1109/ISSPIT.2015.7394341.

11. LI P., YANG Y.X. (2014), Compressed sensing based acoustic data compression and reconstruction technology [in Chinese], *Technical Acoustics*, **33**(1): 14–20.

12. LI S., ZHANG X.P. (2020), A new approach to construct virtual array with increased degrees of freedom for moving sparse arrays, *IEEE Signal Processing Letters*, **27**: 805–809, https://doi.org/10.1109/LSP.2020.2993956.

13. MIRZA H.A., RAJA M.A.Z., CHAUDHARY N.I., QURESHI I.M., MALIK A.N. (2020), A robust multi sample compressive sensing technique for DOA estimation using sparse antenna array, *IEEE Access*, **8**: 140848–140861, https://doi.org/10.1109/ACCESS.2020.3011597.

14. MOHSEN N., HAWBANI A., WANG X.F., AGRAWAL M. (2023), Optimized sparse nested arrays for DoA estimation of non-circular signals, *Signal Processing*, **204**: 108819, https://doi.org/10.1016/j.sigpro.2022.108819.

15. PAL P., VAIDYANATHAN P.P. (2010), Nested arrays: A novel approach to array processing with enhanced degrees of freedom, *IEEE Transactions on Signal Processing*, **58**(8): 4167–4181, https://doi.org/10.1109/TSP.2010.2049264.

16. SALAMA A.A., AHMAD M.O., SWAMY M.N.S. (2020), Compressed sensing DOA estimation in the presence of unknown noise, *Progress in Electromagnetics Research C*, **102**: 47–62, https://doi.org/10.2528/PIERC20031204.

17. SILVER H.W. [Ed.] (2019), *The ARRL Antenna Book*, 24th ed., The American Radio Relay League, Newington.

18. TROPP J.A., GILBERT A.C. (2007), Signal recovery from random measurements via orthogonal matching pursuit, *IEEE Transactions on Information Theory*, **53**(12): 4655–4666, https://doi.org/10.1109/TIT.2007.909108.

19. VAIDYANATHAN P.P., PAL P. (2011), Sparse sensing with co-prime samplers and arrays, [in:] *IEEE Transactions on Signal Processing*, **59**(2): 573–586, https://doi.org/10.1109/TSP.2010.2089682.

20. WANG J. *et al.* (2022), Improved adaptive beamforming algorithm based on compressed sensing [in Chinese], *China Academic Journal Electronic Publishing House*, **38**(5): 18–21+45, https://doi.org/10.16328/j.htdz8511.2022.05.012.

21. YANG Z.X., SHEN Q., LIU W., ELDAR Y.C., CUI W. (2023), High-order cumulants based sparse array design via fractal geometries – Part I: Structures and DOFs, [in:] *IEEE Transactions on Signal Processing*, **71**: 327–342, https://doi.org/10.1109/TSP.2023.3244672.

22. ZHANG X.F. *et al.* (2013), *Array Signal Processing and MATLAB Implementation* [in Chinese], 2nd ed., Publishing House of Electronics Industry, Beijing.

23. ZHAO T., NEHORAI A. (2014), Sparse direction of arrival estimation using co-prime arrays with off-grid targets, [in:] *IEEE Signal Processing Letters*, **21**(1): 26–29, https://doi.org/10.1109/LSP.2013.2289740.